JACS
JOURNAL OF THE AMERICAN CHEMICAL SOCIETY
Communication
pubs.acs.org/JACS

$Li_{10}SnP_2S_{12}$: An Affordable Lithium Superionic Conductor

Philipp Bron,[†,§] Sebastian Johansson,[‡] Klaus Zick,[⊥] Jörn Schmedt auf der Günne,[‡] Stefanie Dehnen,*[,†,§] and Bernhard Roling*[,†,§]

[†]Fachbereich Chemie und Wissenschaftliches Zentrum für Materialwissenschaften (WZMW), Philipps-Universität Marburg, Hans-Meerwein-Straße, 35043 Marburg, Germany

[‡]Inorganic Materials Chemistry, Department of Chemistry/Biology, University of Siegen, 57068 Siegen, Germany

[⊥]Bruker Biospin GmbH, 76287 Rheinstetten, Germany

Supporting Information

ABSTRACT: The reaction of Li_2S and P_2S_5 with $Li_4[SnS_4]$, a recently discovered, good Li^+ ion conductor, yields $Li_{10}SnP_2S_{12}$, the thiostannate analogue of the record holder $Li_{10}GeP_2S_{12}$ and the second compound of this class of superionic conductors with very high values of 7 mS/cm for the grain conductivity and 4 mS/cm for the total conductivity at 27 °C. The replacement of Ge by Sn should reduce the raw material cost by a factor of ∼3.

State-of-the-art lithium-ion batteries utilize liquid electrolytes consisting of $LiPF_6$ dissolved in flammable alkyl carbonates. These electrolytes exhibit a high ionic conductivity around 10 mS/cm at room temperature and a lithium transference number of ∼0.35. However, safety concerns are a major issue. Overheating and overcharging of the battery may lead to a decomposition of the solid electrolyte interface (SEI) and to chemical reactions between electrolyte and electrode materials. The resulting temperature increase may then cause melting of the separator and finally burning of the battery. Therefore, it would be preferable to use exclusively nonvolatile and nonflammable battery materials, especially in the case of high-energy batteries for the automotive sector.[1,2]

Replacing the carbonate-based electrolytes by nonvolatile and thermally stable solid electrolytes is one option that may additionally help to solve other crucial problems of ongoing research, such as short circuits due to lithium dendrite growth on metallic lithium anodes and dissolution of metal ions (e.g., Mn ions)[3] or polysulfide ions[4] from the cathode in the electrolyte. Finally, solid electrolytes offer the possibility to produce multilayer battery structures.[5]

However, apart from the usage of the LIPON solid electrolyte in microbatteries, the integration of solid electrolytes in batteries was strongly hindered by the poor ionic conductivity of most solid lithium ion conductors.[6] In 2011, Kanno et al. reported the synthesis of $Li_{10}GeP_2S_{12}$, a lithium superionic conductor with a conductivity of 12 mS/cm at 27 °C.[7] Since the lithium transference number in this solid electrolyte is essentially unity (electronic conductivity in the range of 10^{-8} to 10^{-9} S/cm),[8] the lithium ion conductivity is even considerably higher than that of the carbonate-based liquid electrolytes. The high conductivity was basically affirmed by MD simulations.[9,10] However, drawbacks for the application in batteries are the scarce deposits and high cost of germanium. Therefore, motivated by our discovery of an already noteworthy conductivity of Li_4SnS_4 ($\sigma_{20\ °C} = 7 \times 10^{-5}$ S/cm),[11] we investigated the possibility to synthesize the thiostannate analogue of the above superionic conductor, namely $Li_{10}SnP_2S_{12}$. On the basis of theoretical studies, Ceder and co-workers suggested this compound to be a possible alternative superionic conductor with lower material cost at similar chemical and electrochemical stability and Li^+ conductivity.[12]

Herein, we report the successful synthesis, the structure, and the ionic conductivity of this material. At 27 °C, the grain lithium ion conductivity is ∼7 mS/cm, and the total conductivity is ∼4 mS/cm. Thus, the total conductivity is similar to that of conventional carbonate-based liquid electrolytes. We emphasize that replacing Ge by Sn should lead to a large reduction of the raw material cost. Considering the current prices for Li_2S, GeS_2, SnS_2 and P_2S_5, the cost for $Li_{10}SnP_2S_{12}$ should only be one-third of that for the germanium analogue.[13]

To obtain $Li_{10}SnP_2S_{12}$, stoichiometric quantities of Li_4SnS_4, Li_2S and P_2S_5 were mixed and ground in an agate mortar, sealed in an evacuated quartz tube, and heated up to 600 °C at a rate of 30 °C/h. The sample was kept for 48 h at 600 °C and slowly cooled down to room temperature (1 °C/h). Purity of the compound was determined by powder X-ray diffraction and TGA/DSC experiments; sample homogeneity was affirmed by EDX measurements and Raman spectra. The latter also served to show the presence of Sn−S and P−S vibrations (see Supporting Information).

As determined by single-crystal X-ray diffraction at 100 K (Figure 1),[14] $Li_{10}SnP_2S_{12}$ is isostructural to the germanium analogue, regarding the space group $P4_2/nmc$ (no. 137) and the atomic positions of the heavy atoms. As in the Ge phase, the tetrel atom shares a position with one of the phosphorus atoms in a statistically disordered 1:1 distribution mode, here leading to a slight elongation of the thermal ellipsoids of S2 and S3 due to different bond lengths, Sn−S and P−S. However, the tin compound displays a different disorder pattern of the lithium atoms with respect to their positions and to the site occupancy factors (sof). The lithium atoms are also distributed over four sites, but we find two Li atoms on 16*h* Wyckoff positions (Li1, Li2, sof 0.50 or 0.30, respectively), one on a 4*d* position (Li3,

Received: July 23, 2013
Published: September 30, 2013

dx.doi.org/10.1021/ja407393y | J. Am. Chem. Soc. 2013, 135, 15694−15697

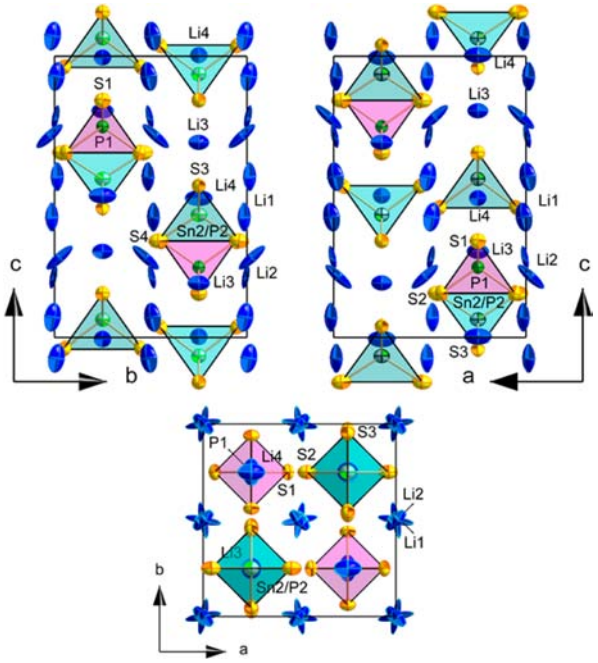

Figure 1. Different views of the single-crystal X-ray structure of $Li_{10}SnP_2S_{12}$. Thermal ellipsoids are drawn at 50% probability. Color code: Li: blue; S: yellow; P: green (disorder of Sn1 and P1 denoted by two-colored representation: gray/green). ES_4 units are shown as pink (P) or green (Sn/P) polyhedra.

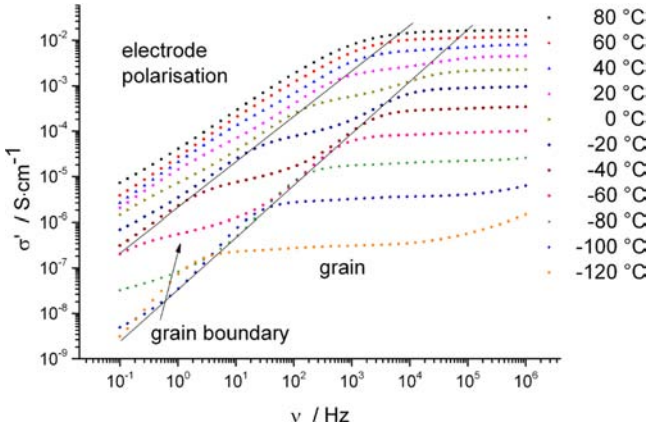

Figure 2. The real part of the conductivity σ' versus frequency ν at different temperatures.

sof 1.00) and the last one on a 4*c* position (Li4, sof 0.80), which is slightly different from the Ge analogue (16*h*, sof 0.47; 4*d*, sof 0.89; 8*f*, sof 0.72; 4*c*, sof 0.77).[15]

All of the 16 partially occupied Li1 positions and all of the 16 partially occupied Li2 positions in the unit cell are situated in channels parallel to the crystallographic *c* axis. The lithium ions on these positions are able to move through the crystal lattice via direct jumps between the (on the average) partially occupied positions without the necessity to make use of unoccupied interstitial sites; they sum up to 6.4 of the total of 10 Li^+ ions per formula unit. Two of the four fully occupied Li3 positions in the unit cell are situated in a channel parallel to the *a* axis, whereas the two remaining occupied Li3 positions fill channels along *b*. These ions thus need to move to unoccupied interstitial positions in order to contribute to the ionic conductivity. All four partially occupied Li4 positions within the unit cell alternate with PS_4 and/or SnS_4 units in *a*, *b* and *c* directions. This coordination environment suggests that Li^+ ions on Li4 positions have to overcome a comparatively large activation barrier to participate in long-range ionic motion. Thus, the short-time ion dynamics should be governed by Li^+ ions on Li1 and L2 positions. However, on millisecond time scales, as probed in PFG-NMR experiments, it is reasonable to expect that all lithium ions interchange their positions and contribute to the ionic conductivity.

The ionic conductivity of annealed pellets was characterized by means of impedance spectroscopy over broad frequency and temperature ranges. To promote good contact between the grains, the pellets were annealed at 500 °C for 12 h prior to the investigation (see Supporting Information for more details). In Figure 2 we show a log−log plot of the real part of the ionic conductivity, σ', versus frequency, ν, at different temperatures. Three different regimes can be distinguished. At low temperatures and high frequencies, the conductivity spectra are governed by Li^+ ion conduction in the crystal grains. At intermediate temperatures and intermediate frequencies, the spectra show dispersion due to the serial impedance of the grain boundaries. At high temperatures and low frequencies, the spectra are governed by electrode polarization due to the usage of ion-blocking electrodes.

It is convenient to analyze the impedance data in a Nyquist plot by fitting the spectra to an equivalent circuit, in which the grain impedance, the grain boundary impedance, and the electrode impedance are represented by circuit elements. From the fit were determined the grain and grain boundary resistances and capacitances (see the Supporting Information for further details). In Figure 3 (bottom) we show Nyquist plots at two different temperatures, T = 153 K and T = 213 K, as an example. At 153 K, the grain semicircle and the high-frequency part of the grain boundary impedance are detected, while at 213 K, the transition from the grain boundary impedance to the electrode impedance is observed.

Figure 4 displays Arrhenius plots of the grain conductivity $\sigma_g = C/R_g$, of the grain boundary conductivity $\sigma_{gb} = C/R_{gb}$, and of the total conductivity $\sigma_{total} = C/(R_g + R_{gb})$. Here, $C = d/A$ is the ratio of the sample thickness d to the sample area A. We note that σ_{gb} is *not* the specific conductivity of the grain boundaries (which can only be calculated in the framework of grain boundary transport models) but rather reflects the contribution of the grain boundaries to the total resistance of the sample. As seen from the figure, both σ_g and σ_{gb} are Arrhenius activated, however with different activation energies, E_A^g = 0.27 eV and E_A^{gb} = 0.60 eV, respectively. Due to the differences in the activation energies and pre-exponential factors, the σ_g and σ_{gb} curves intersect, and the total conductivity curve does not show Arrhenius behavior. Extrapolation of the Arrhenius fit for σ_g to T = 300 K results in a grain conductivity of about 7 mS/cm, whereas the total conductivity at 300 K is about 4 mS/cm.

The diffusion coefficient D of the lithium ions at 298 K was measured by ^{7}Li pulsed field gradient NMR.[16−18] From a plot of the stimulated echo intensity versus the squared gradient amplitude, as shown in Figure 5, a diffusion coefficient $D = 1.8 \times 10^{-12}$ m^2/s was obtained. When we assume that D is determined by diffusion within the grains, we can use the Nernst−Einstein relation (eq 1) to relate the diffusion coefficient to the grain conductivity at 298 K:

dx.doi.org/10.1021/ja407393y | J. Am. Chem. Soc. 2013, 135, 15694−15697

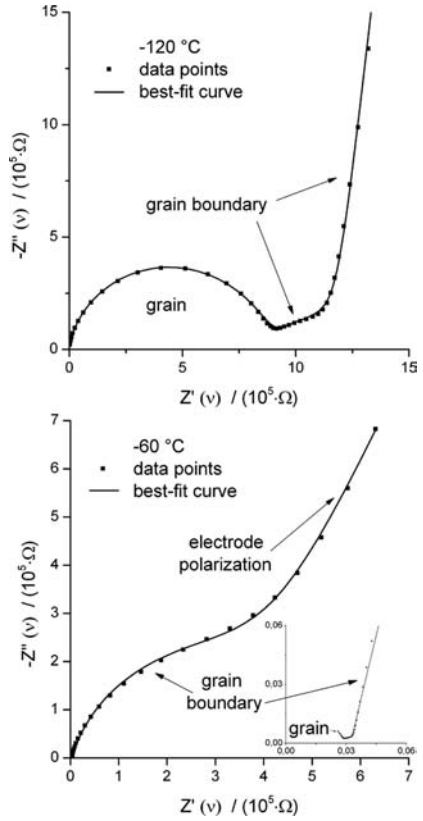

Figure 3. Nyquist plots of the impedance for two different temperatures. The corresponding best-fit curves are displayed as solid lines.

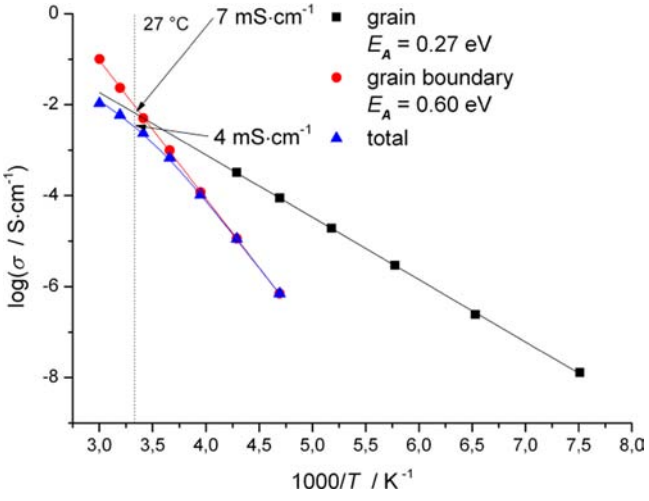

Figure 4. Arrhenius plot of the grain conductivity, grain boundary conductivity, and total conductivity.

$$\sigma_{\text{grain}} = \frac{N_V^{Li^+} \cdot e^2}{k_B \cdot T \cdot H_R} \cdot D \quad (1)$$

with e, k_B, and H_R, denoting the elementary charge, Boltzmann's constant, and the Haven ratio, respectively. From the mass density of the material, ρ = 1.8 g/cm^3, an overall number density of lithium ions of 1.7 × 10^{22} cm^{-3} is obtained. On the NMR time scale, it is reasonable to assume that all Li atoms in the unit cell exchange. Thus, the resulting number density of mobile ions is $N_V^{Li^+}$ = 1.7 × 10^{22} cm^{-3}. Then

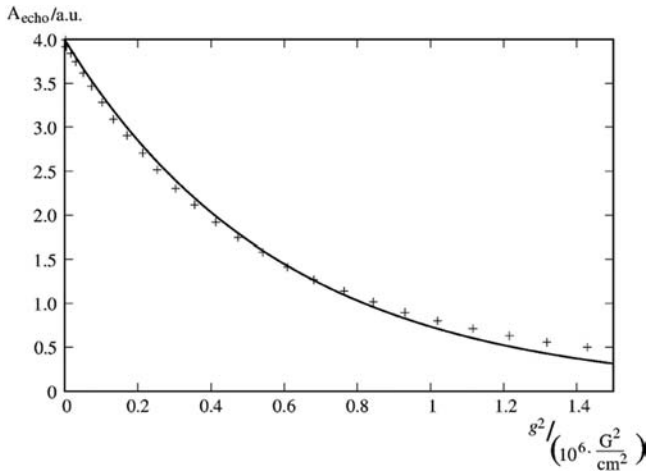

Figure 5. Stimulated echo intensity as a function of the squared gradient amplitude from a ^{7}Li pulsed field gradient NMR experiment.[16,17] A diffusion coefficient of 1.8 × 10^{-12} m^2/s is obtained according to the equation $A_{echo}(g^2) = A \exp[-D\gamma^2\delta^2(\Delta-\delta/3)g^2]$ [18] and based on a Gaussian fit (curved line).

from eq 1, a Haven ratio of ∼0.3 is obtained, which is an expected value for solid electrolytes with high number densities of mobile ions.[19] These results confirm that the measured grain conductivity is indeed caused by very fast lithium ion transport and not by electronic conduction.

In the case of $Li_{10}GeP_2S_{12}$, a total conductivity of 12 mS/cm at 27 °C has been reported, with no distinction made between grain and grain boundary resistance.[8] The high value of the total conductivity together with the Arrhenius behavior observed over the entire temperature range from −140 to 80 °C suggests a negligible contribution of the grain boundary resistance to the total resistance. A comparison with our results reveals that the grain conductivity in $Li_{10}SnP_2S_{12}$ is only slightly lower than in $Li_{10}GeP_2S_{12}$, confirming the predictions of Ceder et al.[12] The comparatively high grain boundary resistance of the thiostannate analogue reduces its total conductivity to 4 mS/cm, but it is assumed that it is possible to reduce the grain boundary resistance by optimization of the annealing conditions. It is noteworthy that even without such a reduction, the total Li^+ ion conductivity of $Li_{10}SnP_2S_{12}$ is essentially identical to that of the standard liquid battery electrolytes.

The high conductivity of the new material, together with the considerably reduced costs due to the replacement of Sn for Ge makes $Li_{10}SnP_2S_{12}$ an attractive and affordable candidate for the application as the electrolyte in solid-state batteries.

■ ASSOCIATED CONTENT

Supporting Information

Further information on characterization and determination of Li^+ conductivity (PXRD, TGA/DSC, EDX, Raman, Impedance and ^{7}Li PFG NMR spectroscopy) and CIF. This material is available free of charge via the Internet at http://pubs.acs.org.

■ AUTHOR INFORMATION

Corresponding Author

dehnen@chemie.uni-marburg.de; roling@staff.uni-marburg.de

Author Contributions

§P.B., S.D. and B.R. contributed equally.

Notes

The authors declare no competing financial interest.

■ ACKNOWLEDGMENTS

This work was supported by the Bundesministerium für Bildung und Forschung (BMBF project, "KoLiWIn" 03SF0343D).

■ REFERENCES

(1) Hammami, A.; Raymond, N.; Armand, M. *Nature* **2003**, *424*, 635.
(2) Masquelier, C. *Nat. Mater.* **2011**, *10*, 649.
(3) Ding, F.; Xu, W.; Graff, G. L.; Zhang, J.; Sushko, M. L.; Chen, X.; Shao, Y.; Engelhard, M. H.; Nie, Z.; Xiao, J.; Liu, X.; Sushko, P. V.; Liu, J.; Zhang, J.-G. *J. Am. Chem. Soc.* **2013**, *135*, 4450.
(4) Wu, X.; Wang, Z.; Li, X.; Guo, H.; Zhang, Y.; Xiao, W. *J. Power Sources* **2012**, *204*, 133.
(5) Ji, L.; Rao, M.; Zheng, H.; Zhang, L.; Li, Y.; Duan, W.; Guo, J.; Cairns, E. J.; Zhang, Y. *J. Am. Chem. Soc.* **2011**, *133*, 18522.
(6) Kato, Y.; Kawamoto, K.; Kanno, R.; Hirayama, M. *Electrochemistry* **2012**, *80*, 749.
(7) Du, Y. A.; Holzwarth, N. A. W. *Phys. Rev. B* **2010**, *81*, 184106.
(8) Kamaya, N.; Homma, K.; Yamakawa, Y.; Hirayama, M.; Kanno, R.; Yonemura, M.; Kamiyama, T.; Kato, Y.; Hama, S.; Kawamoto, K.; Mitsui, A. *Nat. Mater.* **2011**, *10*, 682.
(9) Mo, Y.; Ong, S. P.; Ceder, G. *Chem. Mater.* **2012**, *24*, 15.
(10) Adams, S.; Rao, R. P. *J. Mater. Chem.* **2012**, *22*, 7687.
(11) Kaib, T.; Haddadpour, S.; Kapitein, M.; Bron, P.; Schröder, C.; Eckert, H.; Roling, B.; Dehnen, S. *Chem. Mater.* **2012**, *24*, 2211.
(12) Ong, S. P.; Mo, Y.; Richards, W. D.; Miara, L.; Lee, H. S.; Ceder, G. *Energy Environ. Sci.* **2013**, *6*, 148.
(13) The title compound can be produced in identical quality starting out from Li_4SnS_4 + 3 Li_2S + P_2S_5 or from 5 Li_2S + SnS_2 + P_2S_5. While the first is suitable for lab scale, we recommend the latter for large-scale production.
(14) (a) STOE IPDS2, graphite-monochromatized Mo Ka X-ray, λ = 0.71073 Å, 100 K. Structure solution by direct methods, full-matrix-least-squares refinement against F^2 (SHELXTL).[14] $Li_{10}SnP_2S_{12}$ (M = 634.75 g/mol) tetragonal, $P4_2/nmc$, a/c = 8.7057(4) Å/12.7389(9) Å, V = 965.47(9) Å^3, Z = 2. $R1$ = 0.0366 ($I > 2\sigma(I)$), $wR2$ = 0.0954 (all data), GOF = 0.916. (b) Sheldrick, G. W. *SHELXTL*, 5.1; Bruker AXS Inc.: Madison, WI, 1997.
(15) Kuhn, A.; Köhler, J.; Lotsch, B. V. *Phys. Chem. Chem. Phys.* **2013**, *15*, 11620.
(16) ^{7}Li PFG echo NMR measurement (18, 19) on a Bruker Avance III 600 MHz, using a commercial Bruker Diff50 probe with a maximum gradient of 30 T/m at 25 °C, with the sample sealed in a quartz ampule (ϕ = 10 mm) under Ar.
(17) Tanner, J. E. *J. Chem. Phys.* **1970**, *52*, 5.
(18) Stejskal, E. O.; Tanner, J. E. *J. Chem. Phys.* **1965**, *42*, 288.
(19) Imre, A. W.; Staesche, H.; Voss, S.; Ingram, M. D.; Funke, K.; Mehrer, H. *J. Phys. Chem. B* **2007**, *111*, 5301.